Hindawi Publishing Corporation
VLSI Design
Volume 2008, Article ID 283451, 7 pages
doi:10.1155/2008/283451

*Research Article*

# A Pull-in Based Test Mechanism for Device Diagnostic and Process Characterization

**L. A. Rocha,[1] L. Mol,[2] E. Cretu,[3] R. F. Wolffenbuttel,[2] and J. Machado da Silva[1]**

[1] *1INESC Porto, Faculdade de Engenharia, Universidade do Porto, Rua Dr. Roberto Frias, 4200-465 Porto, Portugal*
[2] *Department of Microelectronics, Faculty of EEMCS, Delft University of Technology, Mekelweg 4, 2628 CD Delft, The Netherlands*
[3] *Department of Electrical and Computer Engineering, University of British Columbia, 2332 Main Mall, Vancouver, BC, Canada V6T 1Z4*

Correspondence should be addressed to L. A. Rocha, lrocha@dei.uminho.pt

Received 17 October 2007; Accepted 26 February 2008

Recommended by Marcelo Lubaszewski

A test technique for capacitive MEMS accelerometers and electrostatic microactuators, based on the measurement of pull-in voltages and resonance frequency, is described. Using this combination of measurements, one can estimate process-induced variations in the device layout dimensions as well as deviations from nominal value in material properties, which can be used either for testing or device diagnostics purposes. Measurements performed on fabricated devices confirm that the 250 nm overetch observed on SEM images can be correctly estimated using the proposed technique.

Copyright © 2008 L. A. Rocha et al. This is an open access article distributed under the Creative Commons Attribution License, which permits unrestricted use, distribution, and reproduction in any medium, provided the original work is properly cited.

## 1. INTRODUCTION

The use of microsystems, containing sensors and actuators, in commercial products calls for simple and automated diagnostics and fault detection mechanisms.Despite the already wide use of these microsystems, their testing techniques tend to be complex and cost-intensive. If on one hand, the complex nature of microsystems, where multiple energy domains interact at the microlevel, imposes an additional level of difficulty, then on the other hand, the large number of fabrication processes available, each of them with their own unique characteristics, makes it difficult to have a process independent test mechanism.

Capacitive accelerometers are among the most commercially available microelectromechanical systems (MEMS), and several built-in self-test (BIST) schemes have been proposed to ensure high-reliability levels [1–4]. In [1], a simple functional test is performed. An electrical test signal is used to stimulate the device, and movement is detected. As this is a very simple functional test, it does not fully evaluates the device, making it unsuitable for more advanced tasks such as diagnostic and manufacturing tests. In [2–4], differential BIST approaches are presented. In [2, 3], the voltage that results from the self-testing operation is used as an indication of asymmetries between capacitors caused by fabrication defects or operational failures, while in [4] a dedicated test signal is applied, and the capacitive readout signal holds information of eventual asymmetries or defects occurring in the device.

A more recent approach [5] proposes the use of the current consumed during a pull-in transition to detect possible failures. Pull-in [6] is a unique feature of capacitive MEMS devices that can provide detailed information about their characteristics. Since the electrostatic force due to a field is inversely proportional to the square of the deflection, and the restoring force of the beam is, to a first approximation, linear with deflection, an unstable system results in case of a deflection, $v$, beyond a critical value, $v_{\mathrm{crit}}$. The pull-in voltage, $V_{\mathrm{pi}}$, is defined as the voltage that is required to obtain this critical deflection and depends mainly on dimensions, residual stress level, and design, which makes it ideal to characterize structural materials in surface micromachining processes [7, 8]. Unlike the case of the comb drive, which is based on area-varying capacitors, the design of most electrostatic actuators relies on gap-width varying capacitors, and the pull-in phenomenon has to be considered [9]. Pull-

in causes the displacement range due to electrostatic forces to be limited to 1/3 of the gap between the electrodes, in case of a motion perpendicular to the capacitor plate orientation.

In this paper, the use of the pull-in voltage as a test parameter is proposed. Furthermore, when pull-in voltage measurements are combined with the measurement of the resonance frequency (a single measurement is needed), the fabrication process nonidealities like overetching and process asymmetries can be estimated. Consecutive pull-in voltage measurements can be used to make accurate diagnostics as well as to perform electronic calibrations.

This paper is organized as follows. Section 2 introduces the pull-in voltage, and in Section 3 the details of the test mechanism are discussed. In Section 4, the test method is evaluated, and a discussion of the experimental results is performed. Finally, in Section 5 some conclusions are presented.

## 2. PULL-IN VOLTAGE

The simplest symmetric micromechanical system suitable for studying the pull-in voltage is composed of three electrodes, one movable and connected to a suspension beam with a certain spring constant $k$ (see Figure 1(a)), and the other two fixed on a rigid supporting substrate. This is often the case of capacitive accelerometers, which have separate electrodes for sensing and actuation.

For a given applied voltage, global stable equilibrium in the microsystem under analysis occurs, if the second derivative of the potential energy of the system with respect to deflection is positive: $\partial^2 U_p/\partial x^2 > 0$. Thus, the pull-in voltage ($V_{\text{pi}}$) results from $\partial^2 U_p/\partial x^2 = 0$ and is determined by the beam material, the beam dimensions, residual stress, and the electrodes dimensions (electrostatic energy). The residual stress should not affect $V_{\text{pi}}$, and therefore the beam should be suspended using folded tethers at each end [10]. This approach ensures that the built-in strain energy component caused by longitudinal stress is negligible.

Due to the symmetry of the structure, three pull-in voltages can be defined as shown in Figure 1(a): asymmetric-right ($V_{\text{pr}}$), asymmetric-left ($V_{\text{pl}}$), and symmetric ($V_{\text{ps}}$). Assuming ideal conditions, analytical expressions for the three pull-in voltages can be found [6]:

$$V_{\text{pr}} = V_{\text{pl}} = \sqrt{\frac{8}{27}\frac{d_0^3 k}{\varepsilon_0 w l}},\qquad V_{\text{ps}} = \sqrt{\frac{1}{2}\frac{d_0^3 k}{\varepsilon_0 w l}}, \tag{1}$$

where $d_0$ is the capacitor initial gap, $k$ is the mechanical spring, $\varepsilon_0 = 8.8546 \times 10^{-12}$ is the air permittivity, and $w$ and $l$ are the capacitor plate width and length, respectively.

If nonideal process conditions are now considered (see Figure 1(b)) like overetching [11], capacitor gap mismatch, and Young's modulus ($E$) value deviations, the pull-in voltage values will vary, making them suitable to estimate the nonidealities and to be used as a diagnostic mechanism.

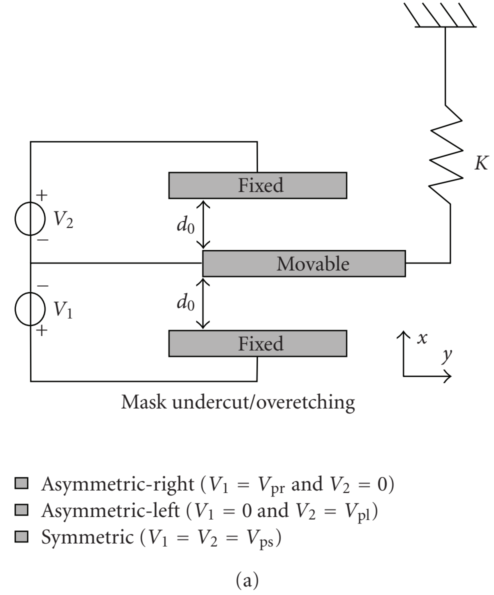


(a)

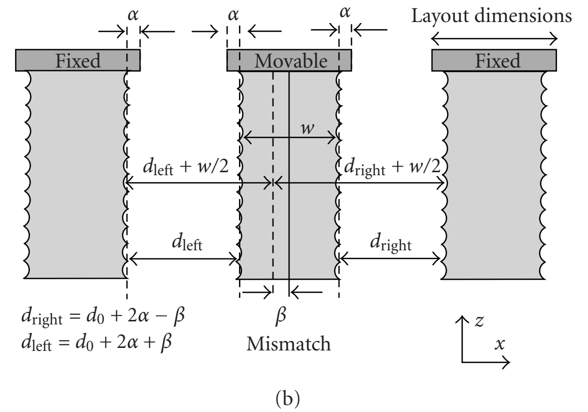


(b)

FIGURE 1: Sketch of the basic device with (a) ideal conditions and (b) with overetch and asymmetries.

## 3. TEST ALGORITHM

The pull-in phenomenon is an intrinsic property of actuated microelectromechanical systems, and therefore it can be used as a test mechanism. Fabricated devices often exhibit smaller dimensions than the actually designed ones (e.g., due to overetching). Overetching can be considered uniform along the microfabricated device [11], which means that all layout dimensions will be affected by the same parameter $\alpha$. This will have a uniform effect on all three pull-in voltages. Small gap mismatches (a few nm) are also observed in fabricated devices. In this case, the gap mismatch ($\beta$) will affect differently the three pull-in voltages and consequently, it becomes easy to estimate $\beta$ from the differences between $V_{\text{pl}}$ and $V_{\text{pr}}$. The parameter $\alpha$ is more difficult to estimate, because there is an extra unknown parameter: the Young's modulus—its average bulk value is known, but it can show large deviations. If we introduce a new measurement, the

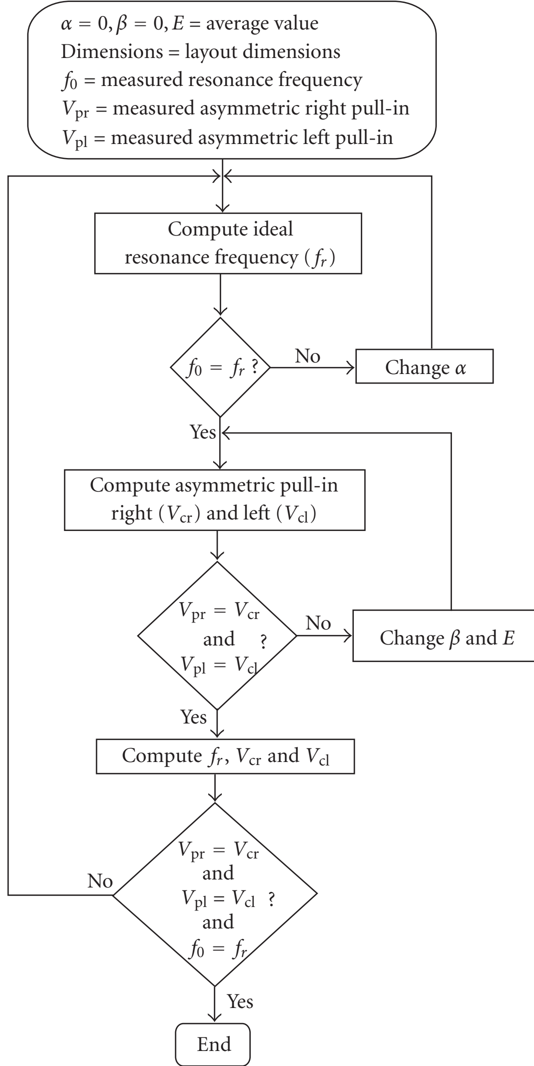


Figure 2: Flow chart to estimate $\alpha$, $\beta$, and $E$ from measurements.

resonance frequency, both $\alpha$ and $E$ can be estimated, and a clear description of the mechanical device is achieved.

A flow chart of the proposed scheme is shown in Figure 2. After this initial estimation, the parameters susceptible of changing with aging and device operations are the Young's modulus and the gap mismatch [12], while the structure dimensions remain constant. This implies that consequent pull-in measurements are an excellent diagnostic parameter. Since the sensitivity of the device is known, test signals can also be applied to the actuation capacitors to calibrate the full system (device plus readout electronics).

One disadvantage of the proposed technique is that it relies on very accurate device models that can predict the device electromechanical behavior. These models have to incorporate all the nonidealities existing in the microdomain, like capacitor fringe fields and residual stress, which makes modeling one of the critical parts of the proposed test scheme.

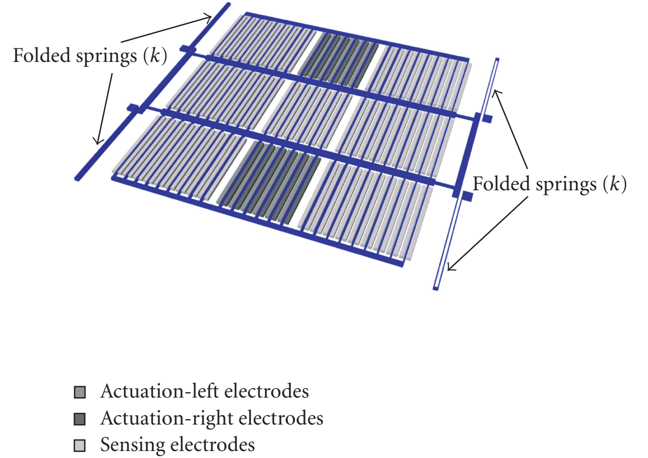


Figure 3: Drawing of the accelerometer.

## 4. EVALUATION OF THE METHOD

Accelerometers fabricated within the Bosch epipoly process [13] were used to evaluate the proposed test scheme. A drawing of the device being used is depicted in Figure 3. Several sets of electrodes are used for sensing while two sets of differential capacitors are used for actuation (left and right).

### 4.1. *Mechanical domain*

The mechanical spring of the structure is composed of 4 folded beams. Assuming that the trusses joining the folded-beam segments are rigid, an approximate analytical expression for $k$ can be found [14]:

$$k(\alpha) = 4\frac{6EI}{(L+2\alpha)^3} = 2Eh\left(\frac{b-2\alpha}{L+2\alpha}\right)^3, \qquad (2)$$

where $I = h(b-2\alpha)^3/12$ is the moment of inertia of the beams, $E$ is the Young's modulus, $\alpha$ is the overetch parameter, and $h$, $b$, and $L$ are the thickness, width and length, respectively, of each beam. A finite-element model (FEM) reveals that this expression overestimates in 4% the actual mechanical spring. This difference is not significant and can be explained by the fact that the analytical model does not consider the bending of the small beam joining the two beams of the folded beam topology.

### 4.2. *Electrical domain*

The device under study has 12 actuation capacitors. The total electrostatic energy can be written as (neglecting fringe fields):

$$U_{\text{elect}}(\alpha) = \frac{1}{2}12C(\alpha)V^2 = \frac{1}{2}12\varepsilon_0\frac{w(l-2\alpha)}{d+2\alpha}V^2, \qquad (3)$$

where $d$ is the capacitor gap distance, $w$ (thickness of the mechanical layer) is the capacitor width, and $l$ is the capacitor length. The analytical (3) does not take into account the

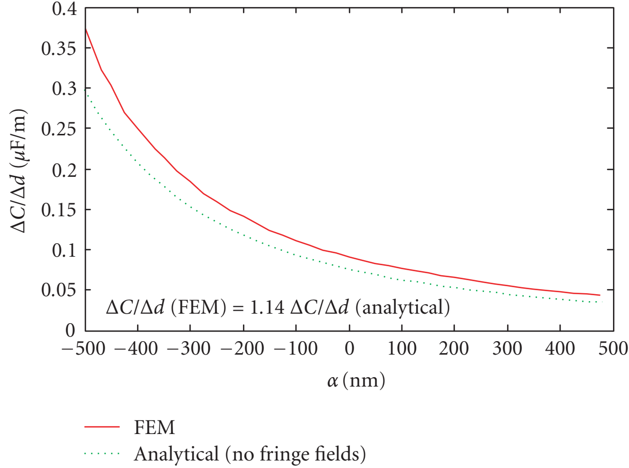


FIGURE 4: Comparison between FEM model and analytical models.

TABLE 1: Main nominal parameters of the device (layout dimensions and bulk material mean values).

| Parameter | Value |
|---|---|
| Spring length ($l$) | 340 $\mu$m |
| Spring width ($b$) | 3 $\mu$m |
| Mechanical layer thickness ($h$) | 10.6 $\mu$m |
| Capacitor length ($l$) | 282 $\mu$m |
| Capacitor width ($w$) | 10.6 $\mu$m |
| Capacitor gap ($d$) | 2 $\mu$m |
| Young's modulus ($E$) | 163 GPa (Poly-Si) |
| Density ($\rho$) | 2.5 g cm$^{-3}$ |

effect of fringe fields, and since in electrostatically actuated MEMS these are very difficult to quantify, numerical methods (FEM) have been used instead. Capacitive FEM simulations for changing $\alpha$ were computed and compared with $(\partial C/\partial d)(\alpha)$. Comparative results are shown in Figure 4, and a small deviation between models can be noticed. The analytical model underestimates the effect of the fringe fields (about 14%). These results prove that fringe-fields contribute to the total electrostatic force and therefore cannot be neglected. The electrostatic force used for the computation of the pull-in voltages is

$$F_{\text{elect}} = 1.14\frac{\partial U_{\text{elect}}(\alpha)}{\partial d}. \quad (4)$$

### 4.3. *Fabricated devices*

The fabricated accelerometers (see Figure 5) are composed of four folded springs, 340 $\mu$m long and 3 $\mu$m wide (layout dimensions), connected to two rigid central bars of about 1 mm long. Parallel-plate capacitors with a 2-$\mu$m gap are used for actuation. The displacement measurement involves sensing the changes of various sets of differential capacitors. The main device layout parameters and bulk material properties are shown in Table 1.

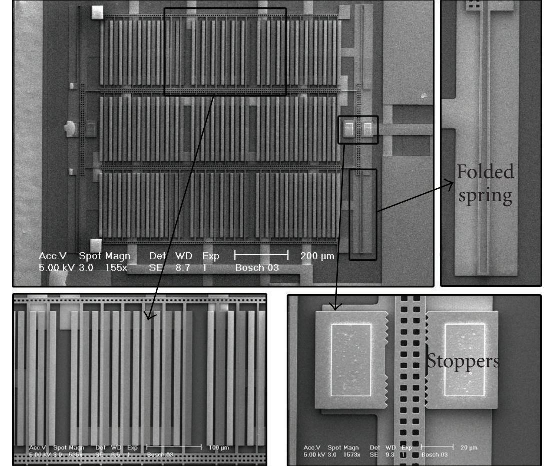


FIGURE 5: Fabricated device.

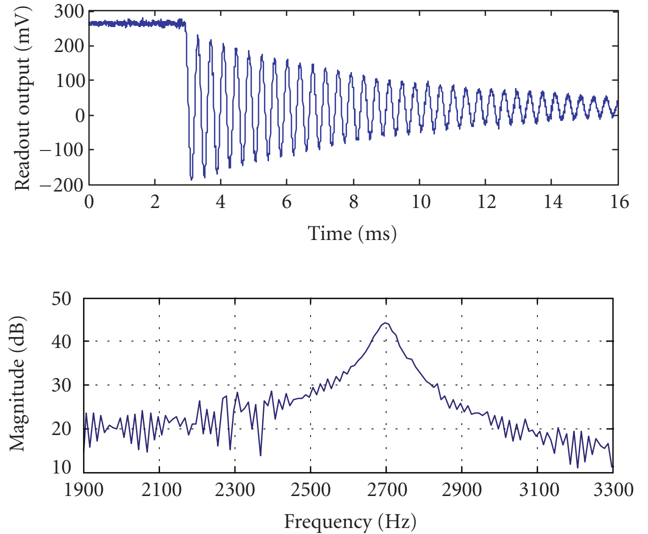


FIGURE 6: Resonance frequency measurements.

### 4.4. *Experimental results*

A batch of 16 devices, fabricated on the same run, was used in the experiments. The devices are encapsulated in vacuum which facilitates the measurement of the resonance frequency. The resonance frequency is determined by acquiring the devices free oscillations followed by a FFT (see Figure 6). The pull-in voltages are retrieved from displacement measurements (see Figure 7) performed while increasing the actuation voltage from zero until an abrupt change is detected. The voltage at which this abrupt change is detected corresponds to the pull-in voltage.

In case of nonfunctional devices, no displacement is observed when actuation voltages are applied. Stiction is detected in devices showing full displacement with no voltage applied.

The measured pull-in voltages showed large deviations (both for asymmetric and symmetric actuation) from device to device, while the deviations between resonance

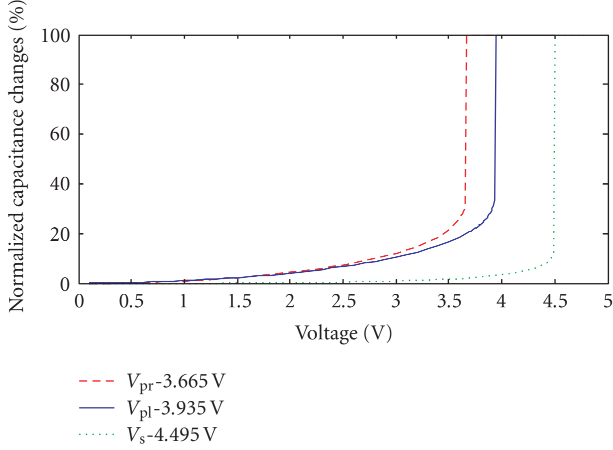


Figure 7: Pull-in measurements.

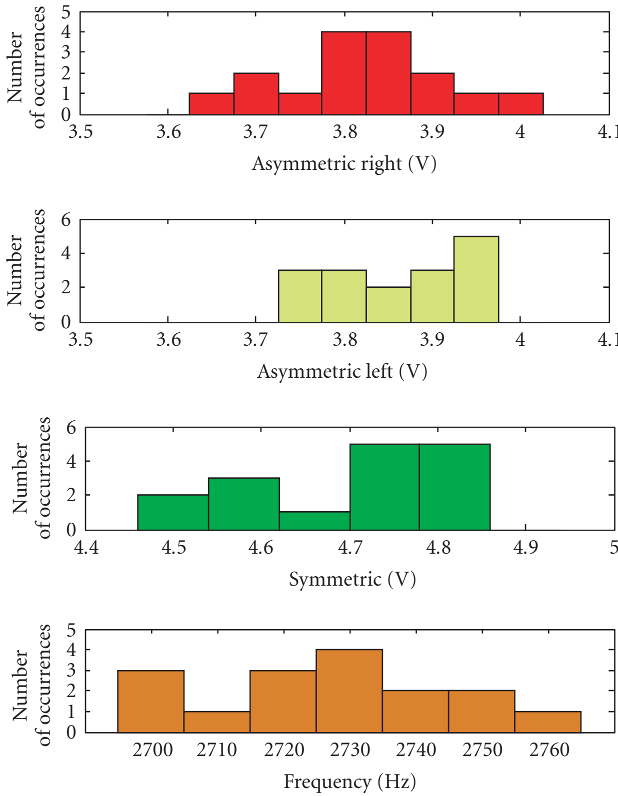


Figure 8: Histogram of the pull-in voltages and resonance frequency measurements.

frequencies were small (ranging from 2700 till 2760 Hz). The experimentally measured values for three of the devices are shown in Table 2. Figure 8 shows the histograms of several measurements that have been performed.

After applying the algorithm of Figure 2 to the set of values retrieved from the measurements, the parameters $\alpha$, $\beta$, and $E$ are estimated. The analytical expressions introduced in the previous subsections are used for the computation of the pull-in voltages. Table 3 presents the estimated values of $\alpha$, $\beta$, Young's modulus, resonance frequency, and pull-in voltages

Table 2: Pull-in and resonance frequency measured values.

| | Parameter | Value |
|---|---|---|
| Device 1 | Asymmetric right-$V_{pr}$ | 3.665 V |
| | Asymmetric left-$V_{pl}$ | 3.935 V |
| | Symmetric-$V_s$ | 4.495 V |
| | Resonance frequency-$f_0$ | 2700 Hz |
| Device 2 | Asymmetric right-$V_{pr}$ | 3.781 V |
| | Asymmetric left-$V_{pl}$ | 3.955 V |
| | Symmetric-$V_s$ | 4.70 V |
| | Resonance frequency-$f_0$ | 2730 Hz |
| Device 3 | Asymmetric right-$V_{pr}$ | 3.751 V |
| | Asymmetric left-$V_{pl}$ | 3.911 V |
| | Symmetric-$V_s$ | 4.679 V |
| | Resonance frequency-$f_0$ | 2720 Hz |

Table 3: Estimated $\alpha$, $\beta$, and $E$ values and simulated pull-in voltages and resonance frequency.

| Device | $\alpha$ | $\beta$ | $E$ | |
|---|---|---|---|---|
| 1 | 253 nm | 60 nm | 142.8 GPa | |
| 2 | 257 nm | 38 nm | 148 GPa | |
| 3 | 255 nm | 35 nm | 145.2 GPa | |
| Device | $V_{pr}$ | $V_{pl}$ | $V_s$ | $f_0$ |
| 1 | 3.665 V | 3.934 V | 4.482 V | 2700 Hz |
| 2 | 3.782 V | 3.956 V | 4.693 V | 2735 Hz |
| 3 | 3.750 V | 3.910 V | 4.665 V | 2716 Hz |

regarding the devices whose measurements are shown in Table 2. Figure 9 shows the histograms of the estimated parameters from all the tested devices. The symmetric pull-in does not contribute with extra information but can be used to confirm the estimated values for $\alpha$, $\beta$, and $E$.

### 4.5. Method verification

The values estimated from the measurements of the 16 devices are in very good agreement ($\alpha$ and $E$ estimated values present a very low standard deviation), which was expected since they all were fabricated in the same run. However, it is interesting to notice that while the estimated values for $\alpha$ and $E$ have a very low standard deviation, the estimated mismatch ($\beta$) values exhibit a large standard deviation. Since the deviations on the pull-in voltages are caused by gap mismatches ($\beta$) and these have influence on device performance, the correct mismatch estimation is one of the strong points of the proposed test approach. The observed mismatches have to do with lateral gradient stresses that often are neglected, or with overetch asymmetries that originate small deviations in the gaps.

In order to verify the estimated average values, some devices were observed using a scanning electron microscope (SEM). Two illustrative SEM images are shown in Figure 10. These SEM images reveal that the devices present an overetching very close to the average one obtained after the test method being proposed. This very good agreement

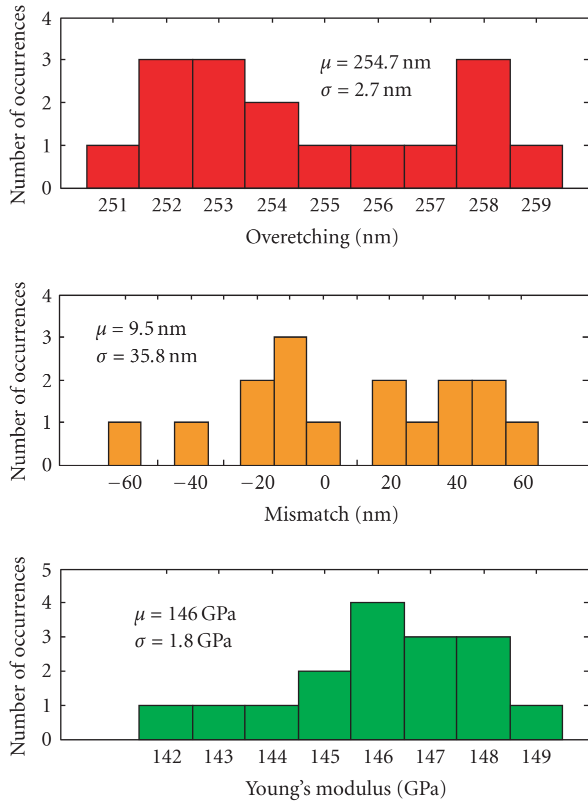


FIGURE 9: Histograms of estimated overetch, mismatch, and Young's modulus obtained from the tested devices.

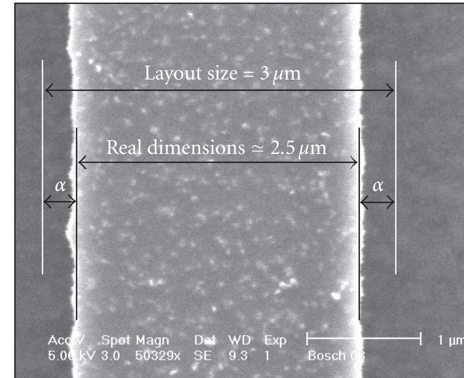


(a)

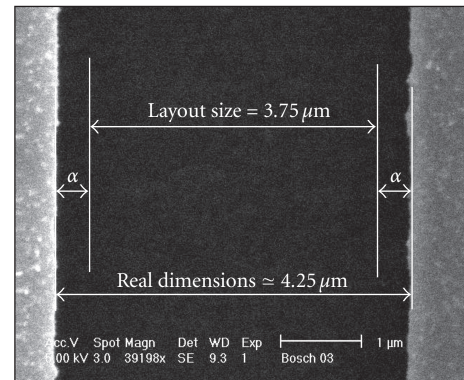


(b)

FIGURE 10: SEM photographs of (a) a folded beam and (b) capacitor gap at the stopper.

proves that pull-in voltage measurements can be used to accurately estimate process deviations and device performance.

### 4.6. Discussion

Like several other MEMS test techniques, the proposed test scheme uses a variable electrical signal to stimulate the device, and the device response can be used to obtain very important device information and most of all to obtain confidence on device functionality (a damaged device will present no pull-in behavior). So far, it has been shown that with this technique the device performance can be characterized but that is not enough to achieve a full BIST technique. Another important parameter in production is testing time. For the measurements presented in this paper, time was not an issue and the pull-in measurements ranged from several seconds to a few minutes (depending on the resolution of the increasing voltage steps used). The minimum achievable test time is directly connected to the dynamics of the device, that is, as the pull-in voltage assumes a quasistatic behavior, the time between steps must guarantee that the device gets to a stable state. Therefore, if a window of 200 mV is considered around the pull-in voltage (the actuation voltages does not start at zero but at a value close to the pull-in expected voltage), with a step resolution of 1 mV and a settling time below 10 milliseconds, a pull-in voltage measurement would require around 2 seconds.

In order to achieve a full BIST technique, on-chip test circuits must be integrated for generating the necessary electrical signals for actuating the device and analyzing the responses. A very simple diagnostic mechanism can be the storage of the initial pull-in voltages on-chip, so that they can be compared with consecutive pull-in voltage measurements. Pull-in voltage deviations from the original values can be used for diagnostic purposes. Before proposing an on-chip test method, long-term measurements must be performed to check and correlate known failure mechanisms with long-term pull-in deviations. First experimental results from the proposed test mechanism prove that the differences between expected pull-in voltages (using layout dimensions) and measured pull-in voltages can be explained from fabrication (overetch, gap mismatches, and Young's modulus deviations). We expect that long-term measurements will be able to give us information on device failures through shifts in the pull-in voltages, and it is likely that different failure modes will present different pull-in deviations in time.

Another advantage of this technique is the fact that it can be used to electrically calibrate an accelerometer. Normal accelerometer calibration (as an example we consider a ±1 g accelerometer) is done by applying a 1 g acceleration followed by a −1 g acceleration (putting the sensitivity axis

along the earth gravity field) while checking the response. Usually, this is done manually and it is not a good solution for remotely placed sensors or sensors with difficult access. Since a very accurate model is obtained with the proposed scheme, the actuation voltages that give the same response as a $\pm 1$ g can be computed and used to electrically calibrate the sensor.

## 5. CONCLUSIONS AND FUTURE WORK

A novel technique is presented which allows estimating over-etching, mismatch, and Young's modulus parameters in capacitive MEMS accelerometers or electrostatic microactuators, relying on the measurement of pull-in voltages and resonance frequency. The underlining theoretical justification is described, and preliminary results obtained with a set of fabricated devices show that results in very good agreement with the expected ones can be obtained, confirming thus the validity of the used MEMS models and the feasibility of the method as a testing technique. The method was tested within a surface micromachining process, but it can be extended to other surface micromachining processes or to more recent technologies like SOI-based processes. The important features are the correctness of the device models and a readout mechanism for pull-in voltage measurements.

In the future, long-term pull-in measurements are needed to check if pull-in deviations from the initial measured values will give information on device's performance deterioration with aging. Future work includes also the identification of failure modes and the estimation of errors due to uncertainty on the measurements and how those can influence the correct estimation of the device parameters.

## REFERENCES

[1] H. V. Allen, S. C. Terry, and D. W. de Bruin, "Accelerometer systems with self-testable features," *Sensors and Actuators*, vol. 20, no. 1-2, pp. 153–161, 1989.

[2] N. Deb and R. D. Blanton, "Built-in self test of CMOS-MEMS accelerometers," in *Proceedings of the International Test Conference (TC '02)*, pp. 1075–1084, Baltimore, Md, USA, October 2002.

[3] N. Deb and R. D. Blanton, "Multi-modal built-in self-test for symmetric microsystems," in *Proceedings of the 22nd IEEE VLSI Test Symposium (VTS '04)*, pp. 139–147, Napa Valley, Calif, USA, April 2004.

[4] X. Xiong, Y.-L. Wu, and W.-B. Jone, "A dual-mode built-in self-test technique for capacitive MEMS devices," in *Proceedings of the 22nd IEEE VLSI Test Symposium (VTS '04)*, pp. 148–153, Napa Valley, Calif, USA, April 2004.

[5] B. Caillard, Y. Mita, Y. Fukuta, T. Shibata, and H. Fujita, "A highly simple failure detection method for electrostatic microactuators: application to automatic testing and accelerated lifetime estimation," *IEEE Transactions on Semiconductor Manufacturing*, vol. 19, no. 1, pp. 35–42, 2006.

[6] L. A. Rocha, E. Cretu, and R. F. Wolffenbuttel, "Analysis and analytical modeling of static pull-in with application to MEMS-based voltage reference and process monitoring," *Journal of Microelectromechanical Systems*, vol. 13, no. 2, pp. 342–354, 2004.

[7] S. T. Cho, K. Najafi, and K. D. Wise, "Internal stress compensation and scaling in ultrasensitive siliconpressure sensors," *IEEE Transactions on Electron Devices*, vol. 39, no. 4, pp. 836–842, 1992.

[8] P. M. Osterberg and S. D. Senturia, "M-TEST: a test chip for MEMS material property measurement using electrostatically actuated test structures," *Journal of Microelectromechanical Systems*, vol. 6, no. 2, pp. 107–118, 1997.

[9] H. A. C. Tilmans and R. Legtenberg, "Electrostatically driven vacuum-encapsulated polysilicon resonators part II. Theory and performance," *Sensors and Actuators A*, vol. 45, no. 1, pp. 67–84, 1994.

[10] W. C. Tang, T.-C. H. Nguyen, and R. T. Howe, "Laterally driven polysilicon resonant microstructures," *Sensors and Actuators*, vol. 20, no. 1-2, pp. 25–32, 1989.

[11] J. V. Clark, D. Garmire, M. Last, J. Demmel, and S. Govindjee, "Practical techniques for measuring MEMS properties," in *Proceedings of the Nanotechnology Conference and Trade Show (NSTI '04)*, vol. 1, pp. 402–405, Boston, Mass, USA, March 2004.

[12] M. Tabib-Azar, K. Wong, and W. Ko, "Aging phenomena in heavily doped ($p^+$) micromachined silicon cantilever beams," *Sensors and Actuators A*, vol. 33, no. 3, pp. 199–206, 1992.

[13] http://www.bosch-sensortec.com/.

[14] J. M. Gere and S. P. Timoshenko, *Mechanics of Materials*, Chapman & Hall, London, UK, 3rd edition, 1991.